

Characterizing the equivalence between dark energy and radiation using gamma-ray bursts

Orlando Luongo^{1,2,3,4,5,*} and Marco Muccino^{1,5,6,†}

¹*University of Camerino, Via Madonna delle Carceri, Camerino, 62032, Italy.*

²*SUNY Polytechnic Institute, 13502 Utica, New York, USA.*

³*INAF - Osservatorio Astronomico di Brera, Milano, Italy.*

⁴*Istituto Nazionale di Fisica Nucleare (INFN), Sezione di Perugia, Perugia, 06123, Italy.*

⁵*Al-Farabi Kazakh National University, Al-Farabi av. 71, 050040 Almaty, Kazakhstan.*

⁶*ICRANet, Piazza della Repubblica 10, 65122 Pescara, Italy.*

Differently from the equivalence time between either matter and radiation or dark energy and matter, the equivalence between dark energy and radiation occurs between two subdominant fluids, since it takes place in the matter dominated epoch. However, dark energy–radiation equivalence may correspond to a *cosmographic bound* since it strongly depends on how dark energy evolves. Accordingly, a possible model-independent bound on this time would give hints on how dark energy evolves in time. In this respect, gamma-ray bursts (GRBs) may be used, in fact, as tracers to obtain cosmic constraints on this equivalence. Consequently, based on observed GR data from the E_p – E_{iso} correlation, we here go beyond by simulating additional GRB data points and investigating two distinct equivalence epochs: 1) dark energy–radiation, and 2) dark energy–radiation with matter. We thus extract constraints on the corresponding two redshifts adopting Monte Carlo Markov chain simulations by means of two methods: the first performing the GRB calibration and the cosmological fit steps independently, and the second performing these steps simultaneously by resorting a hierarchical Bayesian regression. To keep the analysis model-independent, we consider a generic dark energy model, with the unique constraint to reduce to the Λ CDM at $z = 0$. Our findings are thus compared to theoretical predictions, indicating that the Λ CDM model is statistically favored to predict such an equivalence time, though a slow evolution with time cannot be fully excluded. Finally, we critically re-examine the Hubble constant tension in view of our outcomes.

PACS numbers: 98.80.-k, 95.36.+x, 04.50.Kd

Contents

	A. The simulated E_p – E_{iso} data set	7
	B. Calibration of the E_p – E_{iso} correlation	8
I. Introduction		1
II. Equivalence redshifts between dark energy and cosmic fluids		3
A. Model-independent dark energy reconstruction		3
B. Physical meaning of equivalence among cosmological species		3
C. The cosmographic dark energy–matter equivalence redshift		4
D. The cosmographic dark energy–radiation equivalence redshift		5
III. Cosmographic reconstruction of the equivalence redshifts		5
A. Cosmographic bound between dark energy and matter equivalence		5
B. Cosmographic bound between dark energy and radiation equivalence		6
C. Distance reconstructions		6
IV. Forecasting GRB data		6
	V. Cosmological bounds on the equivalence redshifts	8
	A. Numerical constraints: method A	8
	B. Numerical constraints: method B	9
	VI. Theoretical implications of our findings	9
	A. Interpreting <i>cosmographic time discriminator</i>	9
	B. Analyzing the results	10
	VII. Final outlooks and perspectives	11
	Acknowledgements	12
	References	12
	A. Contour plots from Methods A and B	14

I. INTRODUCTION

Dark energy and dark matter constitute the majority of the energy budget of our Universe [1] and their funda-

*Electronic address: orlando.luongo@unicam.it

†Electronic address: marco.muccino@lnf.infn.it

mental nature is still object of heated debate¹.

In the quest to understand dark energy, various hypotheses have been put forth, all seeking to determine whether its equation of state changes with the time [15–18], or if it remains a pure cosmological constant Λ [19]. The latter is generally associated with the effects of primordial quantum fluctuations and represents the key ingredient of the *standard background scenario*, namely the Λ CDM model [20–22], essentially based on six free parameters [1, 23], with the further assumption of flat topology, as supported by various observations² [25].

For its theoretical structure, the Λ CDM model seems to be statistically favored to frame the dark energy dynamics, especially at late and early times. However, cosmological tensions and conceptual issues have been recently raised³ [29], as well as evidence in favor of evolving dark energy even at late times [30].

Consequently, the use of additional standard candles, such as type Ia supernovae (SNe Ia) [31], and/or standard rulers, such as baryonic acoustic oscillations (BAOs) [32], may be not enough to state whether dark energy is dynamical or not. Hence, intermediate- and high-redshift catalogs beyond SN Ia detectability [33] appear crucial to really understand whether the Λ CDM model may be seen as a limiting case of a more general paradigm [34, 35].

Accordingly, GRBs are currently inspected as potential distance indicators [36–40]. Particularly, GRBs may crucially detect deviations from the well-established Λ CDM predictions, clarifying the nature of the aforementioned cosmological tensions.

In this work, we explore the potential use of GRBs to detect limits on the equivalence between dark energy and additional cosmic fluids. Precisely, while the equivalence between matter and radiation applies to very high redshifts, culminating into the *equivalence epoch*, it is challenging to directly constrain either the equivalence between dark energy and radiation or dark energy and matter with radiation⁴. With existing data, these two equivalence times and their corresponding formal periods can be tentatively constrained and, since they are influenced by the dark energy form and free parameters, they can be used to *directly* discriminate among dark energy models and investigate *in a model-independent way* the possible dark energy evolution, representing *de facto* a relatively unexplored subject in the literature. To pursue this goal,

we consider a generic dark energy model that reduces to the Λ CDM paradigm at redshift $z = 0$. Afterwards, we fit our generic model and constrain the equivalence epochs against observed and simulated GRB data points up to very high redshifts, i.e., $z \simeq 12$. To do so, we develop two *model independent* methods: the first performs GRB calibration and cosmological fits *independently*, whereas the second involves a hierarchical Bayesian regression, i.e., performing GRB calibration and cosmological fits *simultaneously*, without passing through the calibration procedure. To do so, we employ Monte Carlo Markov chain (MCMC) fits, utilizing the Metropolis–Hastings algorithm for parameter estimation. The underlying likelihood functions are accordingly maximized under the assumption of Gaussian-distributed errors, with a modified version of the *Wolfram Mathematica* code, originally presented in Ref. [41], whose cosmological applications with GRBs have been extensively tested, see e.g. Refs. [42–45]. Our findings on the dark energy–radiation equivalence time have been computed working out the well-consolidate E_p – E_{iso} correlation of GRBs and indicate that, based on current data, we cannot definitively exclude that dark energy remains constant at very high redshift even at 1 – σ confidence level. However, the predictions of the standard cosmological model consistently fall within the 2 – σ confidence levels, thus certifying that the Λ CDM model may appear statistically favored even at $z \gtrsim 1$. Thus, as a matter of comparison, the results on the equivalence time between dark energy–radiation plus matter, occurring at redshifts extremely close to our time, show the statistical significance of the standard Λ CDM background over generic dark energy model. To confirm this, we also test a w CDM model in both the aforementioned equivalence time domains, thus finding no evident need of having an evolving equation of state, $w \neq -1$. Concluding, our approach is novel since it offers a discerning method towards plausible constraints obtained from the cosmographic equivalence times at different redshift domains. Our findings seem to be in favor of the standard paradigm, matching the criticisms [46–49] against the last developments in favor of a slightly evolving dark energy contribution shown by the DESI collaboration [30]. Finally, we critically re-examine the Hubble constant tension in view of our outcomes, wondering whether our method can be used to acquire more information toward the existence of the H_0 tension itself.

The paper is structured as follows. In Sec. II, we introduce our generic dark energy model, the main features of both model-independent techniques of reconstruction, and how to build up equivalence-time discriminators. Predictions on our priors for different models are thus reported. In Sec. III, the cosmographic reconstructions of our equivalence redshifts have been reported. GRB data from the E_p – E_{iso} correlation are reproduced in Sec. IV. In Sec. V, our numerical results are inferred and critically reinterpreted, and their theoretical interpretation is therefore summarized in Sec. VI, whereas in Sec. VII we develop conclusions and perspectives of our work.

¹ More precisely, dark energy is responsible for present-time cosmic acceleration [2–11], exhibiting repulsive effects [12], while dark matter plays a crucial role in cosmic structure clustering [13, 14].

² The precise determination of spatial curvature Ω_k still remains an open challenge in cosmology [24].

³ For different perspectives about extensions of the standard model, see e.g. Refs. [26–28].

⁴ It is worth to stress that matter–radiation equivalence represents a *cosmological epoch*, i.e., a time before which radiation dominates over other fluids, while equating dark energy with radiation or with radiation plus matter provides *cosmographic redshifts*, without implying a time of domination of one of the two species.

II. EQUIVALENCE REDSHIFTS BETWEEN DARK ENERGY AND COSMIC FLUIDS

In view of the large-scale homogeneity and isotropy of the Universe, the cosmological principle can be reformulated invoking a maximally-symmetric spacetime, represented by the Friedmann-Robertson-Walker (FRW) line element that, in a spatially-flat configuration, reads $ds^2 = dt^2 - a(t)^2 [dr^2 + r^2 (d\theta^2 + \sin^2 \theta d\phi^2)]$. Plugging the metric in Einstein's field equations yields the Friedmann equations,

$$H^2 = \frac{8\pi G}{3} \rho, \quad (1a)$$

$$\dot{H} + H^2 = -\frac{4\pi G}{3} (\rho + 3P), \quad (1b)$$

describing the cosmological dynamics, incorporated in the Hubble parameter $H \equiv \dot{a}/a$, through the energy-momentum components, made up by the total pressure P and density ρ of *each single barotropic fluid*.

Thus, since the total density and pressure appear in the Friedmann equations, the individual subcomponents, constituting ρ and P , cannot be easily *disentangled*, leading *de facto* to a severe *degeneracy problem* [50, 51]. This limitation hampers our understanding of the Universe's dynamics since the crux of the problem lies in the degeneracy between mass and dark energy within the total energy density of the Universe.

To mitigate this issue, we can focus on late and intermediate cosmic evolution, where the total equation of state may be mainly computed through matter, radiation and dark energy contributions.

Consequently, the need of model-independent techniques for cosmological reconstructions, able to disclose information on the Hubble rate derivatives, appear essential [52–56]. Phrasing it differently, cosmological treatments that do not fix the Hubble rate *a priori*, formulating a direct model-independent dark energy reconstruction, turn out to be quite important to characterize dark energy at intermediate redshifts [57, 58].

A. Model-independent dark energy reconstruction

In view of the considerations made above, limiting to matter, radiation and dark energy, the first Friedmann equation acquires the form [59, 60]

$$H(z) = H_0 \sqrt{\Omega_m(1+z)^3 + \Omega_r(1+z)^4 + \Omega_{DE}G(z)}, \quad (2)$$

where $\Omega_m \equiv \rho_m/\rho_c$, $\Omega_r \equiv \rho_r/\rho_c$ and $\Omega_{DE} \equiv \rho_{DE}/\rho_c$, in which $\rho_c \equiv 3H_0^2/(8\pi G)$ is the current value of the critical density and $H_0 = H(z=0)$ is the Hubble constant.

More precisely, in Eq. (2), $G(z)$ is a generic dark energy density, of which we do not explicitly specify the form, and we treat matter and radiation as barotropic fluids,

i.e., starting from their equations of state, $\omega_m = 0$ and $\omega_r = 1/3$, respectively⁵.

To fulfill cosmological constraints, we notably opt for the simplest requirements [59]

$$\begin{cases} G(z) = 1 & , z = 0 \quad , \\ \Omega_{DE} \equiv 1 - \Omega_m - \Omega_r & , \forall z \quad , \\ \Omega_{DE}G(z) \gtrsim \Omega_m(1+z)^3 & , z \rightarrow 0 \quad , \\ \Omega_{DE}G(z) \gtrsim \Omega_r(1+z)^4 & , z \rightarrow 0 \quad , \end{cases} \quad (3)$$

where the second one may directly follow from the first one, whereas the last two properties indicate that at late times dark energy dominates over matter and radiation.

In particular, the latter suggests that, if a cosmological equivalence between dark energy and radiation/matter magnitudes exists, then *it might be present at intermediate epochs*, rather than at current time⁶. Evidently, one may notice that at the equivalence time it must be $G \gtrsim 1$, under the hypothesis that the source for $G(z)$ is a generic barotropic fluid.

Immediately, one can compute the cosmographic terms, namely the deceleration q , the jerk j , and the snap s parameters [68, 69]. In particular, from the definition of the deceleration parameter

$$q(z) = -1 + (1+z) \frac{H'(z)}{H(z)}, \quad (4)$$

having indicated with y' the derivative of y with respect to z , from Eq. (2) we infer

$$q(z) = \frac{1}{2} + \frac{\Omega_r(1+z)^4 + \Omega_{DE}[(1+z)G' - 3G]}{2[\Omega_m(1+z)^3 + \Omega_r(1+z)^4 + \Omega_{DE}G]}, \quad (5a)$$

$$j(z) = (1+z)q'(z) + 2q(z)^2 + q(z), \quad (5b)$$

$$s(z) = -(1+z)j'(z) - j(z)[2 + 3q(z)]. \quad (5c)$$

The above quantities are *general*, above all, *model-independent*, and can be calculated at any redshift, representing the so-called *cosmographic set* [70, 71].

B. Physical meaning of equivalence among cosmological species

At the epoch of matter domination, one can approximate the cosmic fluid with matter and radiation only. Analogously, at current time, one can approximate the universe as composed by matter and dark energy only.

⁵ For a different perspective, involving an effective matter fluid with non-zero pressure, consider Ref. [61–63].

⁶ Around current times, instead, a matter–dark energy equivalence may occur, see Ref. [64] as well as a transition between deceleration and acceleration [65–67].

Consequently, dealing with the equivalence between two fluids implies the existence of a cosmological epoch, namely matter-dominated epoch in the first example, while dark energy-dominated epoch in the second one.

However, since a fluid evolves in time, it is always possible to ensure an equivalence between *any* subdominant fluids. For example, baryons are always subdominant than cold dark matter, but it is clearly possible to presume that the densities of baryons and radiation turn out to be of same order around,

$$z_{br} = -1 + \frac{\Omega_b}{\Omega_r} = 539_{-18}^{+18}, \quad (6)$$

where the baryonic density $\Omega_b = 0.04930_{-0.00086}^{+0.00086}$ and the radiation density $\Omega_r = 9.15_{-0.26}^{+0.26} \times 10^{-5}$ have been considered [1]. However, in the case of Eq. (6), we cannot conclude that a cosmological epoch exists, because at z_{br} the dominant species is the cold dark matter.

Nevertheless, examining the times when two fluids reach equivalence, even if they remain subdominant compared to matter, could provide hints towards their evolution. Thus, the ability to constrain the functional forms of the underlying fluids in a model-independent manner would enable to understand their evolution over time. Accordingly, if we explore the equivalence times between dark energy and other species, albeit such species may not define distinct cosmological epochs, they can still offer clues about dark energy nature. To clarify this point, we first focus on the cosmographic equivalence between dark energy and matter and, later, we pass to the equivalence between dark energy and radiation that will occur during the matter domination epoch.

C. The cosmographic dark energy–matter equivalence redshift

The concept of *equivalence redshift* is frequently associated with the most popular equivalence between radiation and matter, that however occurred in the very early Universe [64, 72], approximately at $z \simeq 10^4$.

However, at intermediate times, there is the need to formulate the existence of a further redshift, roughly corresponding to the *equivalence between dark energy and matter* [64]. This occurs by virtue of the functional form of matter and dark energy. So, one would expect that such an equivalence time can be used rather as a *cosmographic discriminator* toward the understanding of the right cosmological background, *i.e.*, giving hints on the nature of dark energy throughout the Universe evolution. Obtaining possible cosmographic bounds on transition times would therefore clarify whether and how much dark energy evolves.

We here go beyond the standard recipe to search for the equivalence between dark energy and matter, by investigating the redshift, z_{drm} , at which the dark energy density becomes equivalent to the sum of radiation and

matter densities, fulfilling the condition

$$\Omega_{DE} G_{drm} = \Omega_r (1 + z_{drm})^4 + \Omega_m (1 + z_{drm})^3, \quad (7)$$

where hereafter the subscript drm can be written for a generic function as $X_{drm} \equiv X(z_{drm})$.

In particular, this epoch

- may occur at a *smaller redshift* than the transition between dark energy and dark matter;
- differently from the onset of cosmic acceleration, where the deceleration parameter identically vanishes [73], here $q_{drm} \neq 0$. This is an advantage since if one expands q around z_{tr} , the first order is zero and, so, to fix constraints on q one has to reach at least the second order. Instead, for z_{drm} , the first order is not zero and so bounds can be more easily found at first order of Taylor expansion.

To fix priors on our model-independent treatment, we can now provide some forecasts on the equivalence redshifts in the contexts of three well-know background cosmologies [21, 74]:

- the Λ CDM paradigm, with $G^\Lambda(z) = 1$ at all z ,
- the w CDM model with $G^w(z) \equiv (1+z)^{3(1+w)}$, and
- the CPL model [15, 16] with the position $G^{\text{CPL}}(z) \equiv (1+z)^{3(1+w_0+w_1)} \exp[-3w_1 z/(1+z)]$.

Consequently, Eq. (7) for the Λ CDM, w CDM, and CPL scenarios becomes, respectively

$$\Omega_{DE} = \Omega_r (1 + z_{drm})^4 + \Omega_m (1 + z_{drm})^3, \quad (8a)$$

$$G_{drm}^w \Omega_{DE} = \Omega_r (1 + z_{drm})^4 + \Omega_m (1 + z_{drm})^3, \quad (8b)$$

$$G_{drm}^{\text{CPL}} \Omega_{DE} = \Omega_r (1 + z_{drm})^4 + \Omega_m (1 + z_{drm})^3. \quad (8c)$$

Using best-fit values for Λ CDM, w CDM and CPL models [1], from Eqs. (8a)–(8c) the equivalence occurs at

$$z_{drm}^\Lambda = 0.295_{-0.015}^{+0.015}, \quad (9a)$$

$$z_{drm}^w = 0.310_{-0.041}^{+0.050}, \quad (9b)$$

$$z_{drm}^{\text{CPL}} = 0.298_{-0.045}^{+0.063}. \quad (9c)$$

where we used for all the models $\Omega_m = 0.3153_{-0.0073}^{+0.0073}$ and $\Omega_{DE} = 0.6847_{-0.0073}^{+0.0073}$. The additional parameter of the w CDM model is given by $w = -1.028_{-0.031}^{+0.031}$, whereas the additional ones for the CPL parametrization are $w_0 = -0.957_{-0.080}^{+0.080}$ and $w_1 = -0.29_{-0.26}^{+0.32}$.

Thus, the redshifts in Eqs. (9a)–(9c) are easily accessible by fitting the data of low-redshift probes, such as SNe Ia [31], BAOs [32] or cosmic chronometers [75].

Clearly, the above expected values are in quite perfect agreement with the equivalence redshifts between matter and dark energy as obtained e.g. in Ref. [64], indicating that the radiation density parameter is negligible in obtaining bounds with dark energy, as expected. Accordingly, in view of these considerations, in Sec. III A

the contribution of the radiation $\Omega_r(1 + z_{drm})^4$ in the cosmographic reconstruction at the equivalence redshifts z_{drm} will be neglected.

A quite different situation occurs if matter is negligible with respect to radiation. In the case of radiation dominated Universe, assuming that dark energy evolves in the three scenarios indicated before, we will elucidate below which kind of constraints are expected, showing that a possible equivalence between species may occur at much higher redshifts than Eqs. (9a)–(9c).

D. The cosmographic dark energy–radiation equivalence redshift

As stated above, invoking a cosmographic equivalence between dark energy and radiation would

- be strongly dependent on the model under exam,
- discriminate, if computed model-independently, how dark energy behaves at intermediate times,
- occur at higher redshifts than the dark energy - matter equivalence,
- turn out to be less accessible with current data,
- hold likewise $q_{eq} \neq 0$, as for the case of z_{drm} .

Thus, equating dark energy and radiation magnitudes implies a quite different situation than above, accordingly giving through Eq. (2),

$$\Omega_{DE}G_{eq} = \Omega_r(1 + z_{eq})^4. \quad (10)$$

Resorting again the three cosmological models, above described, namely the Λ CDM, w CDM and CPL scenarios, from Eq. (10), we obtain the following constraints

$$\Omega_{DE} = \Omega_r(1 + z_{eq})^4, \quad (11a)$$

$$G_{eq}^w \Omega_{DE} = \Omega_r(1 + z_{eq})^4, \quad (11b)$$

$$G_{eq}^{CPL} \Omega_{DE} = \Omega_r(1 + z_{eq})^4. \quad (11c)$$

Eqs. (11a)–(11b) are solved analytically, whereas Eq. (11c) is solved numerically. Using the already-defined best-fit values for the three scenarios, the equivalence between radiation and dark energy shall occur at

$$z_{eq}^\Lambda = 8.300_{-0.070}^{+0.070}, \quad (12a)$$

$$z_{eq}^w = 7.944_{-0.497}^{+0.551}, \quad (12b)$$

$$z_{eq}^{CPL} = 6.746_{-1.875}^{+4.123}. \quad (12c)$$

Looking at Eqs. (12a)–(12c), we draw the considerations summarized below.

- The equivalence in this case is particularly unstable. Different dark energy paradigms, that degenerate at late times, provide quite different priors on the equivalence redshift, even slightly modifying the free parameters.

- The forecasts span within high-redshift intervals, naively indicating that dark energy scenarios require the use of indicators that cannot be SNe Ia, BAO or OHD data points.

- High-redshift probes like GRBs are the only astrophysical objects placed at intermediate redshifts and able to estimate such redshifts.

In the next section, we shall fix direct bounds on our equivalence redshifts, adopting the aforementioned priors and employing the cosmographic reconstructions, in order to check whether or not the standard cosmological model is predictive enough.

III. COSMOGRAPHIC RECONSTRUCTION OF THE EQUIVALENCE REDSHIFTS

We here consider the simplest dark energy case satisfying the conditions in Eqs. (3). This implies $G_{drm} > 1$ and $G_{eq} > 1$, since both $z_{drm} > 0$ and $z_{eq} > 0$.

We thus single out the cosmographic cases of equivalence among dark energy and matter first, and then dark energy with radiation.

A. Cosmographic bound between dark energy and matter equivalence

This first case occurs at late times, where the equivalence between dark energy and matter happens.

From Eq. (7), neglecting the radiation and fixing $\Omega_{DE} = 1 - \Omega_m$, we obtain

$$z_{drm} = \left[G_{drm} \left(\frac{1 - \Omega_m}{\Omega_m} \right) \right]^{\frac{1}{3}} - 1. \quad (13)$$

Since $\Omega_r \approx 0$ in Eq. (2), then Ω_m can be found by inverting Eq. (13). This procedure is particularly useful as it effectively eliminates the matter density, which typically degenerates with H_0 [76], thereby bypassing the degeneracy problem altogether.

Plugging the expression for Ω_m into Eqs. (5a)–(5c), at z_{drm} we obtain

$$q_{drm} = -\frac{1}{4} + (1 + z_{drm}) \frac{G'_{drm}}{4G_{drm}}, \quad (14a)$$

$$j_{drm} = 1 + \frac{f_{drm}}{4G_{drm}}, \quad (14b)$$

$$s_{drm} = -\frac{5}{4} - (1 + z_{drm}) \frac{G'_{drm}f_{drm} + G_{drm}g_{drm}}{16G_{drm}^2}, \quad (14c)$$

with the definitions

$$f_{drm} \equiv (1 + z_{drm}) [G''_{drm}(1 + z_{drm}) - 2G'_{drm}],$$

$$g_{drm} \equiv 6G'_{drm} + (1 + z_{drm}) [4G'''_{drm}(1 + z_{drm}) - G''_{drm}].$$

We will use the above relations when adopting the GRB data, as we will clarify later.

B. Cosmographic bound between dark energy and radiation equivalence

Following the same argument reported above, from Eq. (10), since $\Omega_{DE} = 1 - \Omega_m - \Omega_r$, it is possible to single out Ω_m . Afterwards, considering Eq. (2) and resorting Eqs. (5a)–(5c), at the equivalence we obtain

$$q_{eq} = \frac{G_{eq} - (1 + z_{eq})^4 \Omega_r - m_{eq}}{g_{eq}}, \quad (15a)$$

$$j_{eq} = -\frac{2(f_{eq} + m_{eq}) - n_{eq}}{g_{eq}}, \quad (15b)$$

$$s_{eq} = -(1 + z_{eq})j'_{eq} - j_{eq}(2 + 3q_{eq}), \quad (15c)$$

where we introduced the following definitions

$$f_{eq} \equiv [2G_{eq} - (1 + z_{eq})^3] \Omega_r,$$

$$g_{eq} \equiv 2[G_{eq}(1 - \Omega_r) + (1 + z_{eq})f_{eq}],$$

$$m_{eq} \equiv [G_{eq} - (1 + z_{eq})^2 G'_{eq}] \Omega_r,$$

$$n_{eq} \equiv [(1 + z_{eq})^3(2z_{eq} - G''_{eq}) - 8G_{eq}z_{eq}] \Omega_r - 2G_{eq}.$$

Again, these relations will be compared with cosmic data and, particularly, with GRBs. We need now to focus on cosmographic reconstructions of distances in order to remove the model-dependence into our computation.

C. Distance reconstructions

Every Hubble rate can be expanded and the derivatives can be compared directly with data points. So, taking Eq. (2) in series of $\Delta z_x = z - z_x$, we write

$$H_{th} = H_x [1 + \mathcal{H}_1^x \Delta z_x + \mathcal{H}_2^x \Delta z_x^2 + \mathcal{H}_3^x \Delta z_x^3], \quad (16)$$

where, depending on the kind of cosmographic reconstruction, “ x ” may indicate either “ drm ” or “ eq ”. At $z = 0$, Eq. (16) constrains to H_0 , yielding [77]

$$H_{th} = H_0 \left[\frac{1 + \mathcal{H}_1^x \Delta z_x + \mathcal{H}_2^x \Delta z_x^2 + \mathcal{H}_3^x \Delta z_x^3}{1 + \mathcal{H}_1^x z_x + \mathcal{H}_2^x z_x^2 + \mathcal{H}_3^x z_x^3} \right], \quad (17)$$

where we baptize

$$\mathcal{H}_1^x = \frac{1 + q_x}{1 + z_x}, \quad \mathcal{H}_2^x = \frac{j_x - q_x^2}{2(1 + z_x)^2}, \quad (18a)$$

$$\mathcal{H}_3^x = \frac{3q_x^2(1 + q_x) - j_x(3 + 4q_x) - s_x}{6(1 + z_x)^3}. \quad (18b)$$

In the above relations, we can utilize the above definitions given in Eqs. (14)–(15).

Once the Hubble rate in Eq. (17) is defined, to explore cosmological bounds over cosmographic reconstructions at the equivalence times, the luminosity distance (in Mpc units) for a spatially-flat Universe can be derived as

$$d_{th}(z) = (1 + z) \int_0^z \frac{dz'}{H_{th}(z')}, \quad (19)$$

providing a simple expression for distance modulus,

$$\mu_{th}(z) = 25 + 5 \log [d_{th}(z)]. \quad (20)$$

The subscript “th” stresses that the here-involved quantities are directly predicted from a *theoretical framework* and, so, unless specified differently later on, appear model-dependent, postulating H_{th} within them.

Bearing Eqs. (19)–(20) with the previous theoretical definition in Eqs. (14)–(15), we now have all the ingredients to employ our cosmic data and perform model-independent analyses as we report below.

IV. FORECASTING GRB DATA

As already mentioned, GRBs are the only astrophysical sources that can probe the Universe at z_{eq} and, possibly, provide useful constraints on the corresponding cosmographic reconstruction [78].

However, in the last two decades, only two bursts lit-up the γ -ray sky at such large distances: GRB 090423 with a spectroscopic redshift $z = 8.2$ [79] and GRB 090429B with a photometric redshift $z \sim 9.4$ [80]. Future missions, among all THESEUS [81], might observe ≈ 100 GRBs at $z \gtrsim 5$ over the first 3 years of activity, with possible detections up to $z \sim 14$ – 15 which would shed light into:

- Universe reionization era, that according to Planck satellite mission is placed around $z = 7.68 \pm 0.79$,
- dark energy–radiation equivalence, placed around $z \simeq 7$ – 9 , as predicted from Eqs. (12a)–(12c).

Hence, forecasting GRB data is needful with the purpose of addressing the lack of GRB data points lying around the redshifts where equivalence occurs.

Consequently, to obtain a more extensive data set of GRBs we can produce a set of both simulated and real observational points, covering a range of redshifts that roughly extends up to $z \simeq 12$.

To do so, we make use of the E_p – E_{iso} correlation, often referred to as the *Amati relation*, [82, 83]

$$\log E_p = a (\log E_{iso} - 52) + b. \quad (21)$$

More precisely, Eq. (21) represents a linear correlation, characterized by a slope a , an intercept b and an extra source of variability σ , established between the GRB spectral peak energy computed in the source rest-frame E_p (in keV units), and the isotropic equivalent energy radiated in γ -rays (in erg units)

$$E_{iso} \equiv 4\pi d_l^2 S_b (1 + z)^{-1}, \quad (22)$$

In Eq. (22) the observed bolometric GRB fluence S_b is determined by integrating the energy spectrum in the rest-frame energy range of 1 – 10^4 keV, whereas d_l denotes the luminosity to the GRB source.

In this analysis, we make use of the most up-to-date catalog of $N_A = 118$ long GRBs from Ref. [84], characterized by a strong correlation between E_p and E_{iso} and the smallest intrinsic dispersion.

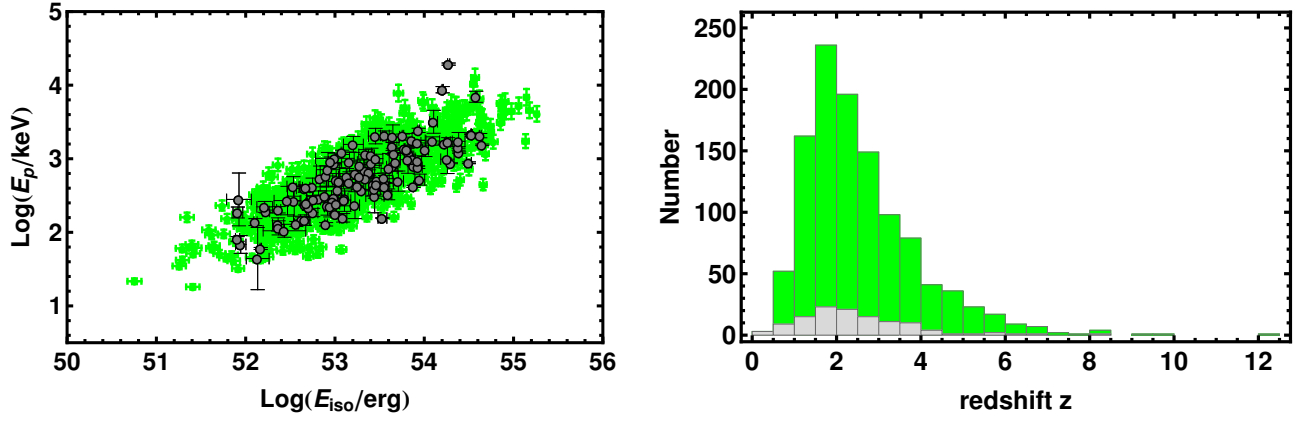


FIG. 1: *Left*: the comparison between the observed $E_{p,i}-E_{iso,i}$ sample [84] (grey data) and the simulated $E_{p,j}-E_{iso,j}$ one (green data). *Right*: the comparison between the distributions of the observed (grey chart) and the simulated (green chart) redshifts.

A. The simulated E_p-E_{iso} data set

In addition to the above N_A sources, we simulate other $N_s = 1000$ GRBs, fulfilling the E_p-E_{iso} correlation. This is motivated by the fact that, with a total number $N = N_A + N_s = 1118$, the overall GRB catalog becomes comparable with the *Pantheon* data set of SNe Ia [31] and with the most updated sample of quasars [85].

As a first step, we need to determine the E_p-E_{iso} correlation parameters (a, b, σ) . We use the Λ CDM paradigm best-fit values [1] to determine the luminosities distances⁷ $d_l(z_i)$ of the observed N_A sources and to compute their isotropic energies $E_{iso}(z_i)$ from Eq. (22).

The correlation parameters can be determined by maximizing the log-likelihood

$$\ln \mathcal{L}_A = - \sum_{i=1}^{N_A} \left\{ \frac{[Y_i - Y(z_i)]^2}{2\sigma_{Y_i}^2} + \ln(\sqrt{2\pi}\sigma_{Y_i}) \right\}, \quad (23)$$

where we defined,

$$Y_i \equiv \log E_{p,i}, \quad (24a)$$

$$Y(z_i) \equiv a [\log E_{iso}(z_i) - 52] + b, \quad (24b)$$

$$\sigma_{Y_i}^2 \equiv \sigma_{\log E_{p,i}}^2 + a^2 \sigma_{\log E_{iso,i}}^2 + \sigma^2. \quad (24c)$$

The corresponding MCMC best-fit parameters are

$$a = 0.537_{-0.039}^{+0.036}, \quad (25a)$$

$$b = 2.043_{-0.055}^{+0.057}, \quad (25b)$$

$$\sigma = 0.257_{-0.018}^{+0.018}. \quad (25c)$$

The simulated data can be built up from the N_A observed GRBs by following the recipe, reported below [86].

- The observed redshifts $\log z_i$ obey a normal distribution characterized by a mean value $\mu_z = 0.359$ and a variance $\sigma_z = 0.214$.
- From the above normal distribution with μ_z and σ_z , we generate N_s redshifts $\log z_j$.
- The observed isotropic energies $\log E_{iso,i}$, in units of 10^{52} erg, follow a normal distribution with a mean value $\mu_E = 1.300$ and a variance $\sigma_E = 0.718$.
- From the above log-normal distribution with μ_E and σ_E , we generate N_s isotropic energies $\log E_{iso,j}$.
- For each pair $(\log z_j, \log E_{iso,j})$ we generate the peak energy $\log E_{p,j}$ from the normal distribution of mean value $\mu_p = a(\log E_{iso,j} - 52) + b$ and variance σ , where (a, b, σ) are taken from Eqs. (25).
- The simulated pairs $(\log E_{p,j}, \log E_{iso,j})$ naturally satisfy the E_p-E_{iso} correlation, once the best-fit parameters, listed in Eqs. (25), are considered.
- The simulated errors on $\log E_{p,j}$ are generated by computing the mean error of the observed peak energies $\langle \sigma_{\log E_{p,i}} \rangle$ and weighting each of them with the ratio of the simulated peak energy and the mean of the observed peak energies $\langle \log E_{p,i} \rangle$, namely

$$\sigma_{\log E_{p,j}} = \langle \sigma_{\log E_{p,i}} \rangle \frac{\log E_{p,j}}{\langle \log E_{p,i} \rangle}. \quad (26)$$
- Similarly, the simulated errors on $\log E_{iso,j}$ are generated by computing the mean error of the observed isotropic energies $\langle \sigma_{\log E_{iso,i}} \rangle$ and the mean of the observed isotropic energies $\langle \log E_{iso,i} \rangle$, namely

$$\sigma_{\log E_{iso,j}} = \langle \sigma_{\log E_{iso,i}} \rangle \frac{\log E_{iso,j}}{\langle \log E_{iso,i} \rangle}. \quad (27)$$

In this respect, Fig. 1 displays the comparison between the observed data set and the simulated catalog (gray

⁷ All the simulated $\log E_{iso,j}$ points are generated using the Λ CDM model. This introduces neither circularity, nor model-dependence issues, as we will show, first introducing the model-independent calibration via Bézier polynomials, and then recalling that $G(z) \rightarrow 1$ as $z \rightarrow 0$, justifying the Λ CDM model use.

versus green points, respectively). In particular, the right plot portrays the redshift distributions of observed and simulated data, evidencing that our initial goal of expanding the data set of GRBs around the likely value of z_{eq} has been achieved with additional 10 additional sources within the range, $7 \lesssim z \lesssim 12$.

B. Calibration of the E_p - E_{iso} correlation

As already noticed from Eq. (22), the isotropic energy measurement is affected by the well-known *circularity problem* [87], meaning that its determination depends upon an *a priori imposition of a background cosmology* due to the luminosity distance d_l .

This issue is overcome only by calibrating E_{iso} by means of model-independent techniques. Here, we resort a well-established strategy, as shown in Refs. [42–45, 88], based on the interpolation of the $N_O = 32$ Hubble rate measurements [75], provided by cosmic chronometers [89], by using a second order Bézier parametric curve,

$$H_2(x) = 100 \left(\frac{\text{km/s}}{\text{Mpc}} \right) \sum_{i=0}^2 2\alpha_i \frac{x^i (1-x)^{2-i}}{i! (2-i)!}, \quad (28)$$

where α_i are the coefficients of the linear combination and the variable $x \equiv z/z_m$ depends upon the maximum redshift $z_m = 1.965$ of the observational Hubble data, obtained from the use of cosmic chronometers.

To estimate the coefficients α_i from cosmic chronometers, we maximize the log-likelihood function,

$$\ln \mathcal{L}_O = - \sum_{k=1}^{N_O} \left\{ \frac{[H_k - H_2(z_k)]^2}{2\sigma_{H_k}^2} + \ln(\sqrt{2\pi}\sigma_{H_k}) \right\}, \quad (29)$$

where the errors σ_{H_k} include the statistical uncertainties [75] and a careful evaluation of the systematic uncertainties [45, 90, 91]. The MCMC best-fit values are

$$\alpha_0 = 0.651_{-0.092}^{+0.091}, \quad (30a)$$

$$\alpha_1 = 1.111_{-0.223}^{+0.219}, \quad (30b)$$

$$\alpha_2 = 2.042_{-0.246}^{+0.248}, \quad (30c)$$

in strict agreement with the results found in Ref. [45].

Bearing in mind the assumption $\Omega_k = 0$ and the results of Eqs. (30), we can obtain a cosmology-independent evaluation of the luminosity distance

$$d_2(z) = (1+z) \int_0^z \frac{dz'}{H_2(z')}, \quad (31)$$

enabling us to obtain a calibrated isotropic energy

$$E_2(z) \equiv 4\pi d_2^2(z) S_b (1+z)^{-1}, \quad (32)$$

where the respective errors on $E_2(z)$ depend on those related to both S_b and $H_2(z)$, propagating to $d_2(z)$.

V. COSMOLOGICAL BOUNDS ON THE EQUIVALENCE REDSHIFTS

Following the guidelines provided above, and using the entire set of observed and simulated GRBs (totaling N), we can determine the correlation parameters (a , b , σ) by assessing a calibration log-likelihood. Simultaneously, we can establish the cosmological parameters at the dark energy – radiation and matter equivalence (h_0 , z_{drm} , G_{drm} , G'_{drm} , G''_{drm} , G'''_{drm}) or at the dark energy – radiation equivalence (h_0 , z_{eq} , Ω_r , G_{eq} , G'_{eq} , G''_{eq} , G'''_{eq}) through a cosmological log-likelihood.

As stated in the introduction, to accomplish this, we employ two methods, conventionally named methods A and B, as described below.

- **Method A** involves the independent maximization of the calibration and cosmological log-likelihood functions using the complete set of N GRBs. Initially, the calibration log-likelihood determines the correlation parameters along with their associated uncertainties. Subsequently, these parameters are utilized in the cosmological log-likelihood to assess the cosmological parameters.
- **Method B**, essentially, is a hierarchical Bayesian regression (HBR). The strategy combines two log-likelihood functions, the first encompassing a calibrator sample of GRBs with redshifts falling within the observational range of cosmic chronometers ($z \leq z_m$), whereas the second consisting of a cosmological sample, comprising the entire GRB dataset.

For the numerical analyses, the subsequent priors on the correlation parameters are assumed,

$$a \in [0, 2], \quad b \in [0, 3], \quad \sigma \in [0, 1],$$

and, analogously, for the cosmographic parameters,

$$\begin{aligned} h_0 &\in [0, 1] & , & & \Omega_r &\in [0, 0.0004] & , \\ z_{drm} &\in [0, 2] & , & & z_{eq} &\in [0, 15] & , \\ G_{drm}, G_{eq} &\in [0, 3] & , & & G'_{drm}, G'_{eq} &\in [-10, 10] & , \\ G''_{drm}, G''_{eq} &\in [-10, 10] & , & & G'''_{drm}, G'''_{eq} &\in [-10, 10] & . \end{aligned}$$

Our findings are thus split for methods A and B.

A. Numerical constraints: method A

Within this approach, the calibration log-likelihood is the same as in Eq. (23) but now it runs over N sources.

In addition, the isotropic energies of the whole sample are now calibrated through the Bézier interpolation, as reported in Eq. (32), and the corresponding errors also account for the uncertainties on $H_2(z)$. Thus, we have

$$Y(z_i) \equiv a [\log E_2(z_i) - 52] + b, \quad (33a)$$

$$\sigma_{Y_i}^2 \equiv \sigma_{\log E_{p,i}}^2 + a^2 \left(\sigma_{\log S_{b,i}}^2 + 4\sigma_{\log d_{2,i}}^2 \right) + \sigma^2. \quad (33b)$$

	a	b	σ	h_0	z_{drm}	–	G_{drm}	G'_{drm}	G''_{drm}	G'''_{drm}
A	$0.537^{+0.017}_{-0.019}$	$2.036^{+0.029}_{-0.023}$	$0.191^{+0.012}_{-0.011}$	$0.846^{+0.149}_{-0.182}$	$0.709^{+0.379}_{-0.420}$	–	$2.678^{+0.313}_{-0.912}$	$-0.395^{+1.333}_{-2.284}$	$-1.896^{+4.191}_{-2.792}$	$0.278^{+3.428}_{-3.280}$
B	$0.708^{+0.018}_{-0.015}$	$1.848^{+0.023}_{-0.030}$	$0.199^{+0.012}_{-0.011}$	$0.701^{+0.176}_{-0.122}$	$0.518^{+0.563}_{-0.288}$	–	$2.709^{+0.291}_{-1.081}$	$0.530^{+1.234}_{-1.592}$	$-3.694^{+4.547}_{-1.190}$	$-1.176^{+4.081}_{-3.361}$
	a	b	σ	h_0	z_{eq}	$10^4 \times \Omega_r$	G_{eq}	G'_{eq}	G''_{eq}	G'''_{eq}
A	$0.537^{+0.017}_{-0.019}$	$2.036^{+0.029}_{-0.023}$	$0.191^{+0.012}_{-0.011}$	$0.825^{+0.079}_{-0.117}$	$5.583^{+3.572}_{-2.093}$	$2.471^{+1.477}_{-1.424}$	$0.968^{+1.328}_{-0.896}$	$-2.711^{+6.046}_{-2.080}$	$3.173^{+1.824}_{-3.840}$	$-1.869^{+5.685}_{-2.836}$
B	$0.727^{+0.017}_{-0.022}$	$1.788^{+0.037}_{-0.028}$	$0.210^{+0.014}_{-0.011}$	$0.712^{+0.086}_{-0.096}$	$7.223^{+1.010}_{-3.264}$	$1.746^{+1.812}_{-0.886}$	$1.628^{+1.094}_{-1.083}$	$3.060^{+1.617}_{-6.502}$	$3.822^{+1.161}_{-8.363}$	$-2.820^{+6.883}_{-1.945}$

TABLE I: Methods A and B best-fit parameters and $1-\sigma$ errors obtained from the whole sample of N GRBs for the cosmographic approaches around dark energy–radiation (top part of Table) and dark energy–matter (bottom part of Table) equivalences.

The MCMC fit for the calibration log-likelihood is the same for both the cosmographic approaches around the dark energy–radiation equivalence and around the dark energy–radiation and matter equivalence. The results are listed in Table I and portrayed in Fig. 2.

The cosmological log-likelihood is given by

$$\ln \mathcal{L}_C = - \sum_{j=1}^N \left\{ \frac{[\mu_j - \mu_{th}(z_j)]^2}{2\sigma_{\mu_j}^2} + \ln(\sqrt{2\pi}\sigma_{\mu_j}) \right\}, \quad (34)$$

where we have resorted the GRB distance moduli obtained from the E_p – E_{iso} correlation and the corresponding errors, respectively [43–45]

$$\mu_j \equiv \frac{5}{2a} \left[\log E_{p,j} - a \log \left(\frac{4\pi S_{b,j}}{1+z_j} \right) - b \right], \quad (35a)$$

$$\sigma_{\mu_j}^2 \equiv \frac{25}{4a^2} \left(\sigma_{\log E_{p,j}}^2 + a^2 \sigma_{\log S_{b,j}}^2 + \sigma^2 \right) + \left(\frac{\partial \mu_j}{\partial a} \right)^2 \sigma_a^2 + 2 \frac{\partial \mu_j}{\partial a} \frac{\partial \mu_j}{\partial b} \sigma_{ab} + \left(\frac{\partial \mu_j}{\partial b} \right)^2 \sigma_b^2, \quad (35b)$$

where σ_a , σ_b and σ_{ab} are the covariance terms between the parameters a and b , needed since the calibration and the cosmological MCMC fits are separately performed.

The results of the MCMC fit for the cosmological log-likelihood, for both cosmographic approaches, are listed in Table I and portrayed in Fig. 2.

B. Numerical constraints: method B

The extrapolation of $H_2(z)$ at $z > z_m$ may bias the calibration of the Amati correlation and, thus, the evaluation of the cosmological parameters [43]. To reduce this possible issue, the HBR combines two nested samples,

- 1) the calibrator sub-sample of GRBs, composed of $N_{cal} = 685$ sources with redshifts $z \leq z_m$, used to estimate the correlation parameters, and
- 2) the cosmological sample, with all the N GRBs, used to estimate the cosmological parameters.

Thus, the total log-likelihood function is given by

$$\ln \mathcal{L} = \ln \mathcal{L}_A + \ln \mathcal{L}_C. \quad (36)$$

For the log-likelihood $\ln \mathcal{L}_A$, the definitions in Eqs. (23) and (33) still hold, with the prescription that the sum runs over the N_{cal} GRBs of the calibrator sub-sample.

The log-likelihood $\ln \mathcal{L}_C$ is the same as in Eq. (34) with the only difference of the distance modulus errors

$$\sigma_{\mu_j}^2 \equiv \frac{25}{4a^2} \left(\sigma_{\log E_{p,j}}^2 + a^2 \sigma_{\log S_{b,j}}^2 + \sigma^2 \right), \quad (37)$$

where the covariance terms σ_a , σ_b and σ_{ab} are no longer needed, since the HBR approach computes a , b and σ together with the other parameters and provides a unique covariance matrix for all the parameters.

The results of the MCMC fits related to the Method B, for both cosmographic approaches around the radiation–dark energy equivalence and around the radiation and matter–dark energy equivalence, are listed in Table I and displayed in Figs. 3 and 4, respectively.

VI. THEORETICAL IMPLICATIONS OF OUR FINDINGS

We here focus on theoretical interpretation and the physical meaning of the two equivalence redshifts, that appear quite different as emphasized in Secs. I and II.

We remark the main differences between inferring a cosmological epoch (where a species dominates) and a cosmographic time discriminator (where two subdominant species equate). Afterwards, the bounds for z_{drm} and z_{eq} , respectively at small and large redshifts, are reported and commented. In this respect, we argue how dark energy may evolve throughout the entire Universe evolution, up to the last simulated GRB redshift bin.

A. Interpreting cosmographic time discriminator

When we equate the magnitudes of matter, radiation, and dark energy, we can get evidence for the existence of distinct cosmological epochs, characterized by varying combinations of the three mentioned components.

As stated in Sec. II, a cosmological epoch arises when a given constituent dominates over the other cosmic fluids at a given time. Examples are the equivalences between matter and radiation and/or dark energy with matter.

The underlying approximation is valid when we consider an Einstein-de Sitter Universe, in which one fluid only drives the overall cosmological dynamics.

Conversely, computing the equivalence between dark energy and radiation magnitudes would imply the same as above only if there exists an epoch where radiation dominates over dark energy and a subsequent time where dark energy dominates over radiation. However, the presence of matter complicates this scenario and, in fact, at redshift $z \simeq 7-10$, as predicted by Eqs. (12a)–(12c), radiation is significantly less dominant than matter.

Consequently, dark energy and radiation magnitudes can be the same, but matter would dominate over them and, in turn, we cannot deal with a proper cosmological epoch, but rather with a cosmographic time that discriminates how and whether dark energy is dynamical. Phrasing it differently, we seek a *cosmographic time discriminator* associated with the form of dark energy.

Clearly, this process is identified under certain circumstances, such as,

- there is no interaction among constituents, i.e., no interactions between dark energy and radiation, or between dark energy and matter and so forth occur,
- the fluids evolve with precise equations of state,
- dark energy does not increase dramatically as the Universe expands,
- no early dark energy has been postulated,
- spatial curvature is negligible throughout the Universe's history and does not influence the analysis.

The last condition deserves a better clarification. While, spatial curvature does not have a substantial impact on the equivalence at low redshifts, around $z \lesssim 1$, its influence may become more pronounced as z increases.

All these theoretical considerations justify the focus on our two equivalences: one at very low redshifts, involving dark energy with matter plus radiation, and the subsequent equivalence between dark energy and radiation.

B. Analyzing the results

Method A. The results of the MCMC fits are summarized in Table I and portrayed in Fig. 2. We recall that method A performs calibration and cosmological fits separately, thus neglecting the hierarchy of the log-likelihood functions and the mutual influence of both correlation and cosmological parameters. This is particularly evident looking at the bounds on the cosmographic parameters.

- **Equivalence at z_{drm} .** With respect to the Λ CDM predictions, the cosmographic parameters h_0 , z_{drm} and G_{drm} exhibit quite high values. However, if on the one hand h_0 and z_{drm} are consistent with the concordance model due to the huge attached errors, on the other G_{drm} is incompatible with the

expectation $G(z) = 1$, though its derivatives within the huge errors are consistent with the cosmological constant conjecture.

- **Equivalence at z_{eq} .** In this epoch, h_0 and z_{eq} are, respectively, higher and lower than (but within the errors consistent with) the concordance model values. The resulting Ω_r parameter is higher and barely inconsistent with the value provided by the Planck satellite [1]. Conversely, G_{eq} and its derivatives are consistent – within huge errors – with the standard cosmological constant scenario.

Method B. The results of the MCMC are listed in Table I and portrayed in Figs. 3 and 4.

- **Equivalence at z_{drm} .** The values of h_0 and z_{drm} are still higher but closer to those predicted by the Λ CDM model. Further, G_{drm} is here incompatible with the concordance model.
- **Equivalence at z_{eq} .** In this case, within large errors, all the parameters are consistent with the cosmological concordance background.

From the results of the two methods, we draw the conclusions listed below.

- The Bayesian approach provides improved results with respect to the method A, in particular on z_{eq} .
- The epoch z_{drm} provides the most controversial constraint in both methods, i.e., $G_{drm} > 1$. This may be seen as a direct consequence of the shortage of low-redshift GRBs. Even including the N_s simulated GRBs, the number of sources at $z \lesssim 0.6$ is just 10, too scarce to obtain acceptable and reliable constraints for the equivalence at low redshifts.
- The sample of GRBs is large enough to provide constraints that are in line with the expectations of the concordance paradigm.

In view of these outcomes, we notice that contrasting conclusions may arise in view of the *dark energy evolution* and the *Hubble constant tension*.

- **Equivalence at z_{drm} .** For both the methods, the results suggest $G_{drm} > 1$ with null derivatives. Both sets of constraints are consistent with the dark energy under the form of a constant or of a slowly evolving function of time (nearly constant). On the other hand, the large attached errors do not provide enough elements for a definitive conclusion.
- **Equivalence at z_{eq} .** Conversely to z_{drm} , G_{eq} and its derivatives favor the cosmological constant scenario. However, the large errors cannot firmly exclude the possibility that dark energy may slowly evolve with time, as well as for the z_{drm} case.

In addition, it is worth noticing what follows.

- The results of the equivalence epoch at z_{drm} are jeopardized by the lack of sources at low redshift, preventing us to obtain reliable estimates.
- Though not conclusive, the above considerations tend to favor the cosmological constant scenario purported by the Λ CDM paradigm.
- The Hubble constant tension is not fully-addressed, since all values of h_0 in Table I are consistent, within the errors, with both Planck estimate in the flat scenario [1] and $h_0 = 0.7304 \pm 0.0104$ inferred from Cepheids [92]. It is worth noticing that Method B results are in line with a recent estimate got from SNe Ia based on surface brightness fluctuations measurements, i.e., $h_0 = 0.7050 \pm 0.0237$ [93], that seems to indicate that the Hubble constant may be in between the extreme values currently in mutual tension. So, even though our methods are model-independent, the existing tension is far from reaching its solution even adopting GRBs.

Finally, we compare our findings with those of Ref. [64] and summarized the implications of the current work.

- We went further in the cosmographic reconstruction of dark energy equation of state, up to $G'''(z)$.
- We investigated such a reconstruction also for the high-redshift equivalence epoch at z_{eq} .
- We utilized only GRBs to provide constraints on the two equivalence epochs.
- We did not include the spatial curvature in our analysis for mainly two reasons: first the calibration of GRB data with the interpolation of the Hubble rate data is not straightforward when the spatial curvature is accounted for, and, second, in Ref. [64], it was shown that its inclusion did not significantly change the results.

VII. FINAL OUTLOOKS AND PERSPECTIVES

In this work we investigated the cosmic reconstructions of two different equivalence epochs between dark energy and a) radiation and b) radiation and matter.

We discussed the physical meaning of these two epochs. Then, we distinguished the equivalence as a cosmological epoch, where one of the two fluids dominates over all the others, from the equivalence between two subdominant fluids. In the latter, we introduced the concept of cosmographic time discriminator, showing that this equivalence may serve as discriminator among cosmological models.

To work this procedure out, we selected GRB data from the well-consolidated E_p-E_{iso} correlation. To overcome the *circularity problem* [87], GRB data were calibrated through the well-established Bézier interpolation

of the Hubble rate measurements [42–45, 88]. GRBs represent unique astrophysical sources that lap z_{eq} and future missions, such as THESEUS [81], will provide wider numbers of GRB detections at $z \gtrsim 5$, i.e., considerably increasing the catalog and possibly helping in shedding light around the equivalence epochs here considered. In this respect, for consistency, we used GRBs alone also for getting bounds on the low-redshift equivalence at z_{drm} .

However, to increase the statistic and the quality of our constraints, we simulated 1000 additional GRBs fulfilling the E_p-E_{iso} correlation so that the redshift coverage spans up to $z \simeq 12$. In particular, we showed that if an equivalence between subdominant species like dark energy and radiation occurs, then it happens in the matter-dominated era, i.e., at $z \gtrsim 7$, being strongly dependent on the free parameters of a given dark energy model.

In this respect, we considered two kind of MCMC fitting methods to extract cosmic bounds: in the first, GRB calibration and cosmological fits are performed independently, whereas in the second, essentially a hierarchical Bayesian regression, are performed simultaneously.

The outcomes of our analysis showed that:

- Method B provided better results than method A. However, both outcomes appeared more in line with the expectations of the concordance paradigm, in particular for the z_{eq} bounds.
- The value $G_{drm} > 1$ implied a larger value of z_{drm} , though consistent with the Λ CDM scenario, within the error bars. This issue is very likely due to shortage of GRBs (observed and simulated) at low redshifts that affects the bounds got from the cosmographic reconstruction during this epoch.
- Besides the above issue resulting in $G_{drm} > 1$ at z_{drm} , both methods indicated that dark energy is mainly in the form of a cosmological constant or slightly evolving with time. Precisely, the bounds from the equivalence at z_{eq} are more in line with the concordance model expectations though. However, the large attached errors did not provide enough elements for a definitive conclusion.
- The Hubble constant tension was not fully-fixed, albeit the more trustworthy results, got from the equivalence at z_{eq} , provided bounds that seemed to indicate that the Hubble constant may lie between the well-known two values measured in Refs. [1, 92].

Summarizing, our outcomes, though non-conclusive, confirmed the general trend that the Λ CDM model is the most suited one to describe the cosmic evolution, at least with the current level of precision of GRB data.

Certainly, as perspectives, new and more precise data from GRB surveys can improve the situation, especially for accessing the high-redshift domains. Indeed, our simulated GRB data reflect the current level of accuracy for GRB observables and include also the additional errors

(both statistical and systematic) of the Hubble rate measurements, introduced by the calibration procedure.

Nevertheless, to compensate the lack of low-redshift GRBs and improve cosmographic reconstructions around z_{drm} , it is desirable to include also low-redshift catalogs such as SNe Ia, Hubble rate measurements, BAOs and so on, and find the most suited technique to combine them.

As a final hint, we will use our methods to check more complicated dark energy scenarios, even involving plausible interactions among dark constituents and/or adding the spatial curvature as well. Further, the results provided by the DESI mission [30] will be included to refine the analysis and to check whether departures on the equivalence times will be expected.

Acknowledgements

The authors are grateful to Kuantay Boshkayev and Peter K. S. Dunsby for very useful discussions on the topic of cosmological models. OL is thankful to Alejandro Aviles, Francesco Pace and Sunny Vagnozzi for intriguing debates on the nature of dark energy and on the impact of the last cosmological findings toward a possible evolution of dark energy. MM acknowledges Lorenzo Amati, Massimo Della Valle, Luca Izzo and Luca Porcelli for valuable comments on the numerical analyses.

-
- [1] Planck Collaboration, *A&A* **641**, A6 (2020), 1807.06209.
- [2] S. Perlmutter, G. Aldering, M. della Valle, S. Deustua, R. S. Ellis, S. Fabbro, A. Fruchter, G. Goldhaber, D. E. Groom, I. M. Hook, et al., *Nature* **391**, 51 (1998), *astro-ph/9712212*.
- [3] A. G. Riess, A. V. Filippenko, P. Challis, A. Clocchiatti, A. Diercks, P. M. Garnavich, R. L. Gilliland, C. J. Hogan, S. Jha, R. P. Kirshner, et al., *AJ* **116**, 1009 (1998), *astro-ph/9805201*.
- [4] S. Perlmutter, G. Aldering, G. Goldhaber, R. A. Knop, P. Nugent, P. G. Castro, S. Deustua, S. Fabbro, A. Goobar, D. E. Groom, et al., *ApJ* **517**, 565 (1999), *astro-ph/9812133*.
- [5] J. L. Tonry, B. P. Schmidt, B. Barris, P. Candia, P. Challis, A. Clocchiatti, A. L. Coil, A. V. Filippenko, P. Garnavich, C. Hogan, et al., *ApJ* **594**, 1 (2003), *astro-ph/0305008*.
- [6] S. L. Bridle, O. Lahav, J. P. Ostriker, and P. J. Steinhardt, *Science* **299**, 1532 (2003), *astro-ph/0303180*.
- [7] C. L. Bennett, M. Halpern, G. Hinshaw, N. Jarosik, A. Kogut, M. Limon, S. S. Meyer, L. Page, D. N. Spergel, G. S. Tucker, et al., *ApJ Suppl. Ser.* **148**, 1 (2003), *astro-ph/0302207*.
- [8] G. Hinshaw, D. N. Spergel, L. Verde, R. S. Hill, S. S. Meyer, C. Barnes, C. L. Bennett, M. Halpern, N. Jarosik, A. Kogut, et al., *ApJ Suppl. Ser.* **148**, 135 (2003), *astro-ph/0302217*.
- [9] A. Kogut, D. N. Spergel, C. Barnes, C. L. Bennett, M. Halpern, G. Hinshaw, N. Jarosik, M. Limon, S. S. Meyer, L. Page, et al., *ApJ Suppl. Ser.* **148**, 161 (2003), *astro-ph/0302213*.
- [10] D. N. Spergel, L. Verde, H. V. Peiris, E. Komatsu, M. R.olta, C. L. Bennett, M. Halpern, G. Hinshaw, N. Jarosik, A. Kogut, et al., *ApJ Suppl. Ser.* **148**, 175 (2003), *astro-ph/0302209*.
- [11] D. J. Eisenstein, I. Zehavi, D. W. Hogg, R. Scoccamarro, M. R. Blanton, R. C. Nichol, R. Scranton, H.-J. Seo, M. Tegmark, Z. Zheng, et al., *ApJ* **633**, 560 (2005), *astro-ph/0501171*.
- [12] O. Luongo and H. Quevedo, *Phys. Rev. D* **90**, 084032 (2014), 1407.1530.
- [13] L. Bergstrom, *New J. Phys.* **11**, 105006 (2009), 0903.4849.
- [14] S. Profumo, L. Giani, and O. F. Piattella, *Universe* **5**, 213 (2019), 1910.05610.
- [15] M. Chevallier and D. Polarski, *International Journal of Modern Physics D* **10**, 213 (2001), gr-qc/0009008.
- [16] E. V. Linder, *Physical Review Letters* **90**, 091301 (2003), *astro-ph/0208512*.
- [17] P. J. Peebles and B. Ratra, *Reviews of Modern Physics* **75**, 559 (2003), *astro-ph/0207347*.
- [18] A. L. King, T. M. Davis, K. D. Denney, M. Vestergaard, and D. Watson, *MNRAS* **441**, 3454 (2014), 1311.2356.
- [19] T. Padmanabhan, *Phys. Rep.* **380**, 235 (2003), *hep-th/0212290*.
- [20] V. Sahni and A. Starobinsky, *International Journal of Modern Physics D* **9**, 373 (2000), *astro-ph/9904398*.
- [21] E. J. Copeland, M. Sami, and S. Tsujikawa, *International Journal of Modern Physics D* **15**, 1753 (2006), *hep-th/0603057*.
- [22] S. Tsujikawa, in *Astrophysics and Space Science Library*, edited by S. Matarrese, M. Colpi, V. Gorini, and U. Moschella (2011), vol. 370 of *Astrophysics and Space Science Library*, p. 331, 1004.1493.
- [23] L. Perivolaropoulos and F. Skara, *arXiv e-prints arXiv:2105.05208* (2021), 2105.05208.
- [24] J. Ooba, B. Ratra, and N. Sugiyama, *ApJ* **864**, 80 (2018), 1707.03452.
- [25] G. Efstathiou and S. Gratton, *MNRAS* **496**, L91 (2020), 2002.06892.
- [26] O. Luongo and M. Muccino, *Phys. Rev. D* **98**, 103520 (2018), 1807.00180.
- [27] R. D'Agostino, O. Luongo, and M. Muccino, *Classical and Quantum Gravity* **39**, 195014 (2022), 2204.02190.
- [28] A. Belfiglio, R. Giambò, and O. Luongo, *arXiv e-prints arXiv:2206.14158* (2022), 2206.14158.
- [29] J.-P. Hu and F.-Y. Wang, *Universe* **9**, 94 (2023), 2302.05709.
- [30] DESI Collaboration, *arXiv e-prints p. arXiv:2404.03002* (2024), 2404.03002.
- [31] D. M. Scolnic, D. O. Jones, A. Rest, Y. C. Pan, R. Chornock, R. J. Foley, M. E. Huber, R. Kessler, G. Narayan, A. G. Riess, et al., *ApJ* **859**, 101 (2018), 1710.00845.
- [32] A. Cuceu, J. Farr, P. Lemos, and A. Font-Ribera, *JCAP* **2019**, 044 (2019), 1906.11628.
- [33] S. A. Rodney, A. G. Riess, D. M. Scolnic, D. O. Jones, S. Hemmati, A. Molino, C. McCully, B. Mobasher, L.-G.

- Strolger, O. Graur, et al., *AJ* **150**, 156 (2015).
- [34] S. Capozziello, R. D'Agostino, and O. Luongo, *International Journal of Modern Physics D* **28**, 1930016 (2019), 1904.01427.
- [35] S. Capozziello, R. D'Agostino, and O. Luongo, *MNRAS* **494**, 2576 (2020), 2003.09341.
- [36] M. Muccino, L. Izzo, O. Luongo, K. Boshkayev, L. Amati, M. Della Valle, G. B. Pisani, and E. Zaninoni, *ApJ* **908**, 181 (2021), 2012.03392.
- [37] S. Cao, M. Dainotti, and B. Ratra, *MNRAS* **512**, 439 (2022), 2201.05245.
- [38] O. Luongo and M. Muccino, *Galaxies* **9**, 77 (2021), 2110.14408.
- [39] M. G. Dainotti, G. Sarracino, and S. Capozziello, *Publ. Astr. Soc. Japan* (2022), 2206.07479.
- [40] X. D. Jia, J. P. Hu, J. Yang, B. B. Zhang, and F. Y. Wang, arXiv e-prints arXiv:2208.09272 (2022), 2208.09272.
- [41] R. Arjona, W. Cardona, and S. Nesseris, *Phys. Rev. D* **99**, 043516 (2019), 1811.02469.
- [42] L. Amati, R. D'Agostino, O. Luongo, M. Muccino, and M. Tantalò, *MNRAS* **486**, L46 (2019), 1811.08934.
- [43] O. Luongo and M. Muccino, *MNRAS* **503**, 4581 (2021), 2011.13590.
- [44] O. Luongo and M. Muccino, *MNRAS* **518**, 2247 (2023), 2207.00440.
- [45] M. Muccino, O. Luongo, and D. Jain, *MNRAS* **523**, 4938 (2023), 2208.13700.
- [46] A. C. Alfano, O. Luongo, and M. Muccino, arXiv e-prints arXiv:2411.04878 (2024), 2411.04878.
- [47] A. C. Alfano, O. Luongo, and M. Muccino, arXiv e-prints arXiv:2408.02536 (2024), 2408.02536.
- [48] Y. Carloni, O. Luongo, and M. Muccino, arXiv e-prints arXiv:2404.12068 (2024), 2404.12068.
- [49] O. Luongo and M. Muccino, *A&A* **690**, A40 (2024), 2404.07070.
- [50] A. Aviles and J. L. Cervantes-Cota, *Phys. Rev. D* **84**, 083515 (2011), [Erratum: *Phys.Rev.D* **84**, 089905 (2011)], 1108.2457.
- [51] R. von Martens, L. Lombriser, M. Kunz, V. Marra, L. Casarini, and J. Alcaniz, *Phys. Dark Univ.* **28**, 100490 (2020), 1911.02618.
- [52] O. Luongo and M. Muccino, *Mon. Not. Roy. Astron. Soc.* **518**, 2247 (2022), 2207.00440.
- [53] A. Aviles, J. Klapp, and O. Luongo, *Phys. Dark Univ.* **17**, 25 (2017), 1606.09195.
- [54] L. Izzo, O. Luongo, and S. Capozziello, *Mem. Soc. Astron. Ital. Suppl.* **19**, 37 (2012), 1011.1151.
- [55] A. Aviles, C. Gruber, O. Luongo, and H. Quevedo, *Phys. Rev. D* **86**, 123516 (2012), 1204.2007.
- [56] P. K. S. Dunsby and O. Luongo, *Int. J. Geom. Meth. Mod. Phys.* **13**, 1630002 (2016), 1511.06532.
- [57] F. S. N. Lobo, J. P. Mimoso, and M. Visser, *JCAP* **2020**, 043 (2020), 2001.11964.
- [58] R. W. Tucker, D. A. Burton, and A. Noble, *General Relativity and Gravitation* **37**, 1555 (2005), gr-qc/0411131.
- [59] O. Luongo, G. B. Pisani, and A. Troisi, *Int. J. Mod. Phys. D* **26**, 1750015 (2016), 1512.07076.
- [60] S. Capozziello, R. D'Agostino, and O. Luongo, *Phys. Dark Univ.* **36**, 101045 (2022), 2202.03300.
- [61] O. Luongo and M. Muccino, *Phys. Rev. D* **98**, 103520 (2018), 1807.00180.
- [62] A. Belfiglio, Y. Carloni, and O. Luongo, *Physics of the Dark Universe* **44**, 101458 (2024), 2307.04739.
- [63] A. Belfiglio, O. Luongo, and T. Mengoni, arXiv e-prints arXiv:2411.11130 (2024), 2411.11130.
- [64] A. C. Alfano, C. Cafaro, S. Capozziello, and O. Luongo, *Physics of the Dark Universe* **42**, 101298 (2023), 2306.08396.
- [65] A. Melchiorri, L. Pagano, and S. Pandolfi, *Phys. Rev. D* **76**, 041301 (2007), 0706.1314.
- [66] A. C. Alfano, S. Capozziello, O. Luongo, and M. Muccino, *Journal of High Energy Astrophysics* **42**, 178 (2024), 2402.18967.
- [67] S. Capozziello, P. K. S. Dunsby, and O. Luongo, *MNRAS* **509**, 5399 (2022), 2106.15579.
- [68] P. K. S. Dunsby and O. Luongo, *International Journal of Geometric Methods in Modern Physics* **13**, 1630002-606 (2016), 1511.06532.
- [69] M. Visser, *Gen. Rel. Grav.* **37**, 1541 (2005), 0411131.
- [70] M. Visser, Cattoën, and C. , in *Dark Matter in Astrophysics and Particle Physics, Dark 2009*, edited by H. V. Klapdor-Kleingrothaus and I. V. Krivosheina (2010), pp. 287–300, 0906.5407.
- [71] C. Cattoën and M. Visser, *Classical and Quantum Gravity* **24**, 5985 (2007), 0710.1887.
- [72] M. Muccino, L. Izzo, O. Luongo, K. Boshkayev, L. Amati, M. Della Valle, G. B. Pisani, and E. Zaninoni, *Astrophys. J.* **908**, 181 (2021), 2012.03392.
- [73] C. J. A. P. Martins and M. Prat Colomer, *A&A* **616**, A32 (2018), 1806.07653.
- [74] M. Li, X.-D. Li, S. Wang, and Y. Wang, *Front. Phys. (Beijing)* **8**, 828 (2013), 1209.0922.
- [75] D. Kumar, D. Jain, S. Mahajan, A. Mukherjee, and A. Rana, *International Journal of Modern Physics D* **32**, 2350039 (2023), 2205.13247.
- [76] C. Rubano and P. Scudellaro, arXiv e-prints astro-ph/0203225 (2002), astro-ph/0203225.
- [77] O. Luongo, In preparation (2025).
- [78] O. Luongo and M. Muccino, *Galaxies* **9**, 77 (2021), 2110.14408.
- [79] N. R. Tanvir, D. B. Fox, A. J. Levan, E. Berger, K. Wiersema, J. P. U. Fynbo, A. Cucchiara, T. Krühler, N. Gehrels, J. S. Bloom, et al., *Nature* **461**, 1254 (2009), 0906.1577.
- [80] A. Cucchiara, A. J. Levan, D. B. Fox, N. R. Tanvir, T. N. Ukwatta, E. Berger, T. Krühler, A. Küpcü Yıldız, X. F. Wu, K. Toma, et al., *ApJ* **736**, 7 (2011), 1105.4915.
- [81] L. Amati, P. T. O'Brien, D. Götz, E. Bozzo, A. Santangelo, N. Tanvir, F. Frontera, S. Mereghetti, J. P. Osborne, A. Blain, et al., *Experimental Astronomy* **52**, 183 (2021), 2104.09531.
- [82] L. Amati, F. Frontera, M. Tavani, J. J. M. in't Zand, A. Antonelli, E. Costa, M. Feroci, C. Guidorzi, J. Heise, N. Masetti, et al., *A&A* **390**, 81 (2002), astro-ph/0205230.
- [83] L. Amati and M. Della Valle, *International Journal of Modern Physics D* **22**, 1330028 (2013), 1310.3141.
- [84] N. Khadka, O. Luongo, M. Muccino, and B. Ratra, *JCAP* **2021**, 042 (2021), 2105.12692.
- [85] G. Risaliti and E. Lusso, *Nature Astronomy* **3**, 272 (2019), 1811.02590.
- [86] L.-X. Li, *MNRAS* **379**, L55 (2007), 0704.3128.
- [87] Y. Kodama, D. Yonetoku, T. Murakami, S. Tanabe, R. Tsutsui, and T. Nakamura, *MNRAS* **391**, L1 (2008), 0802.3428.
- [88] A. Montiel, J. I. Cabrera, and J. C. Hidalgo, *MNRAS* **501**, 3515 (2021), 2003.03387.

- [89] R. Jimenez and A. Loeb, *ApJ* **573**, 37 (2002), [astro-ph/0106145](#).
- [90] M. Moresco, R. Jimenez, L. Verde, A. Cimatti, and L. Pozzetti, *ApJ* **898**, 82 (2020), [2003.07362](#).
- [91] M. Moresco, L. Amati, L. Amendola, S. Birrer, J. P. Blakeslee, M. Cantiello, A. Cimatti, J. Darling, M. Della Valle, M. Fishbach, et al., *Living Reviews in Relativity* **25**, 6 (2022), [2201.07241](#).
- [92] A. G. Riess, W. Yuan, L. M. Macri, D. Scolnic, , D. Brout, et al., *ApJ Lett.* **934**, L7 (2022), [2112.04510](#).
- [93] N. Khetan, L. Izzo, M. Branchesi, R. Wojtak, M. Cantiello, C. Murugesan, A. Agnello, E. Cappellaro,

M. Della Valle, C. Gall, et al., *A&A* **647**, A72 (2021), [2008.07754](#).

Appendix A: Contour plots from Methods A and B

We here show the contour plots obtained from MCMC analyses of Methods A and B for both the cosmographic approaches around the dark energy–radiation and dark energy–radiation and matter equivalences.

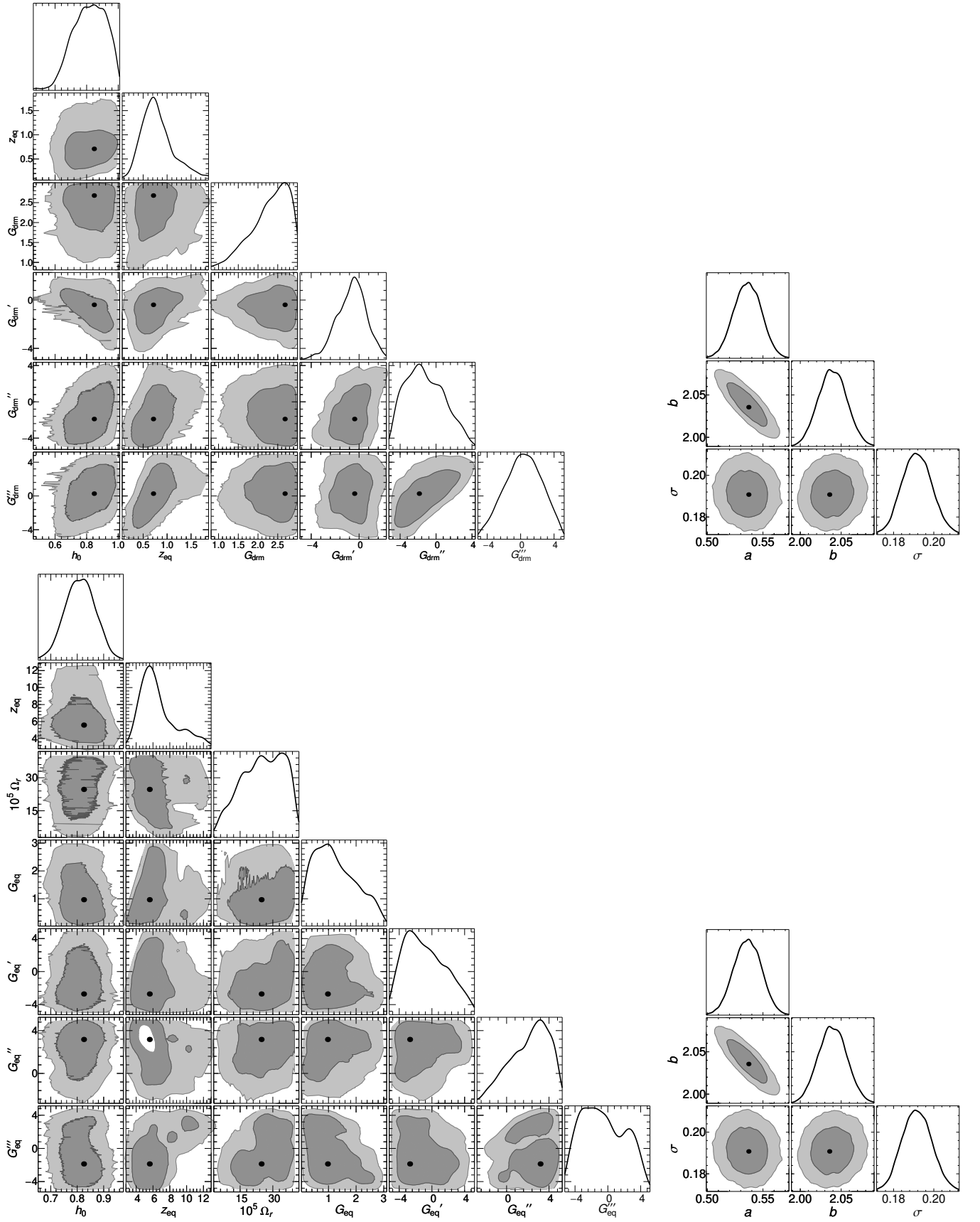


FIG. 2: Method A contour plots from the calibrated $E_{\text{p}}-E_{\text{iso}}$ correlation. *Top panels*: the best-fit parameters at the dark energy – matter and radiation equivalence. *Bottom panels*: the best-fit parameters at the dark energy – radiation equivalence. Darker (lighter) areas mark the $1-\sigma$ ($2-\sigma$) confidence regions.

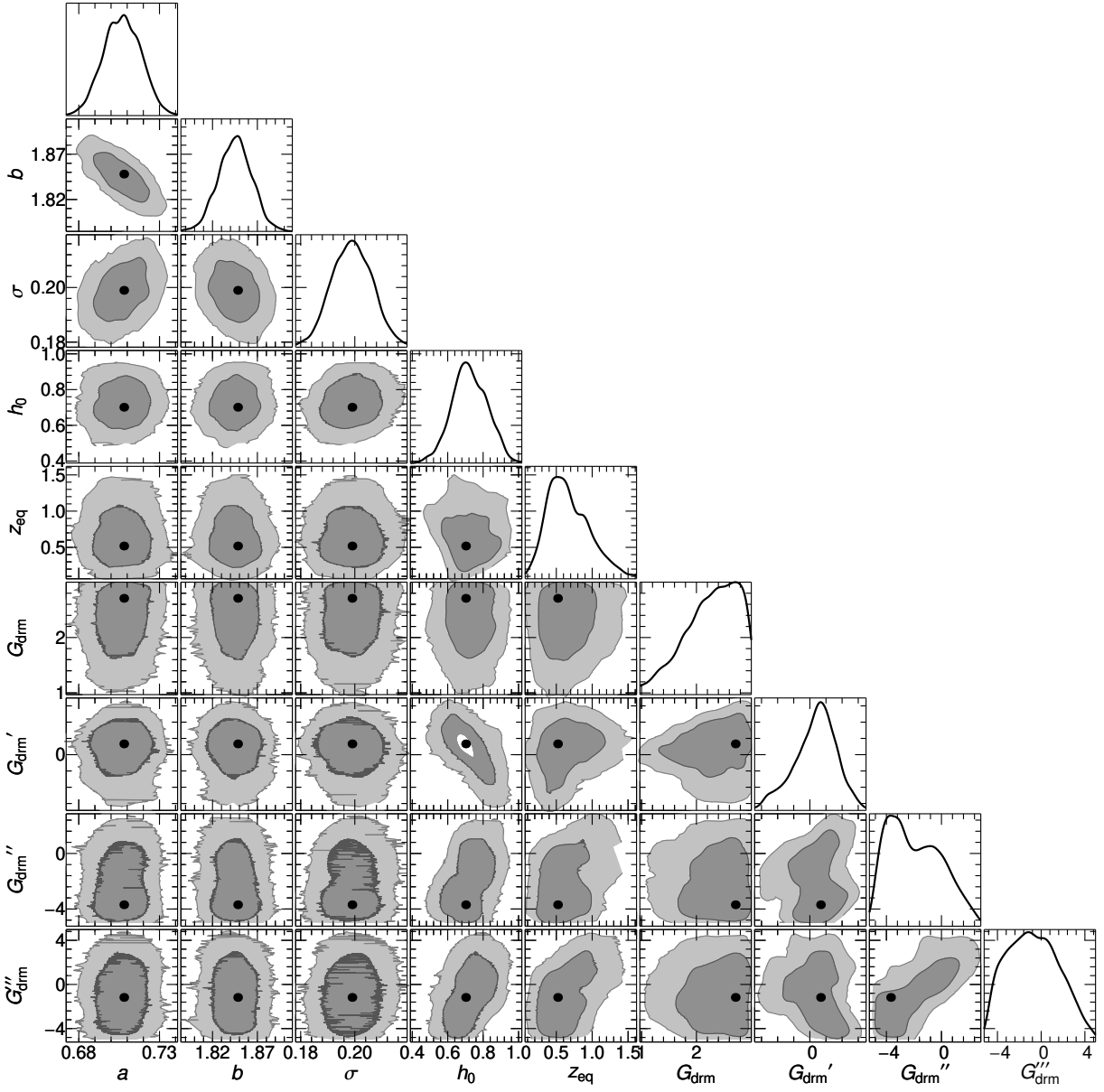


FIG. 3: Method B contour plots, got from the HBR technique, of the best-fit parameters of the E_p-E_{iso} correlation and the cosmographic approach at the dark energy – matter and radiation equivalence. Darker (lighter) areas mark the $1-\sigma$ ($2-\sigma$) confidence regions.

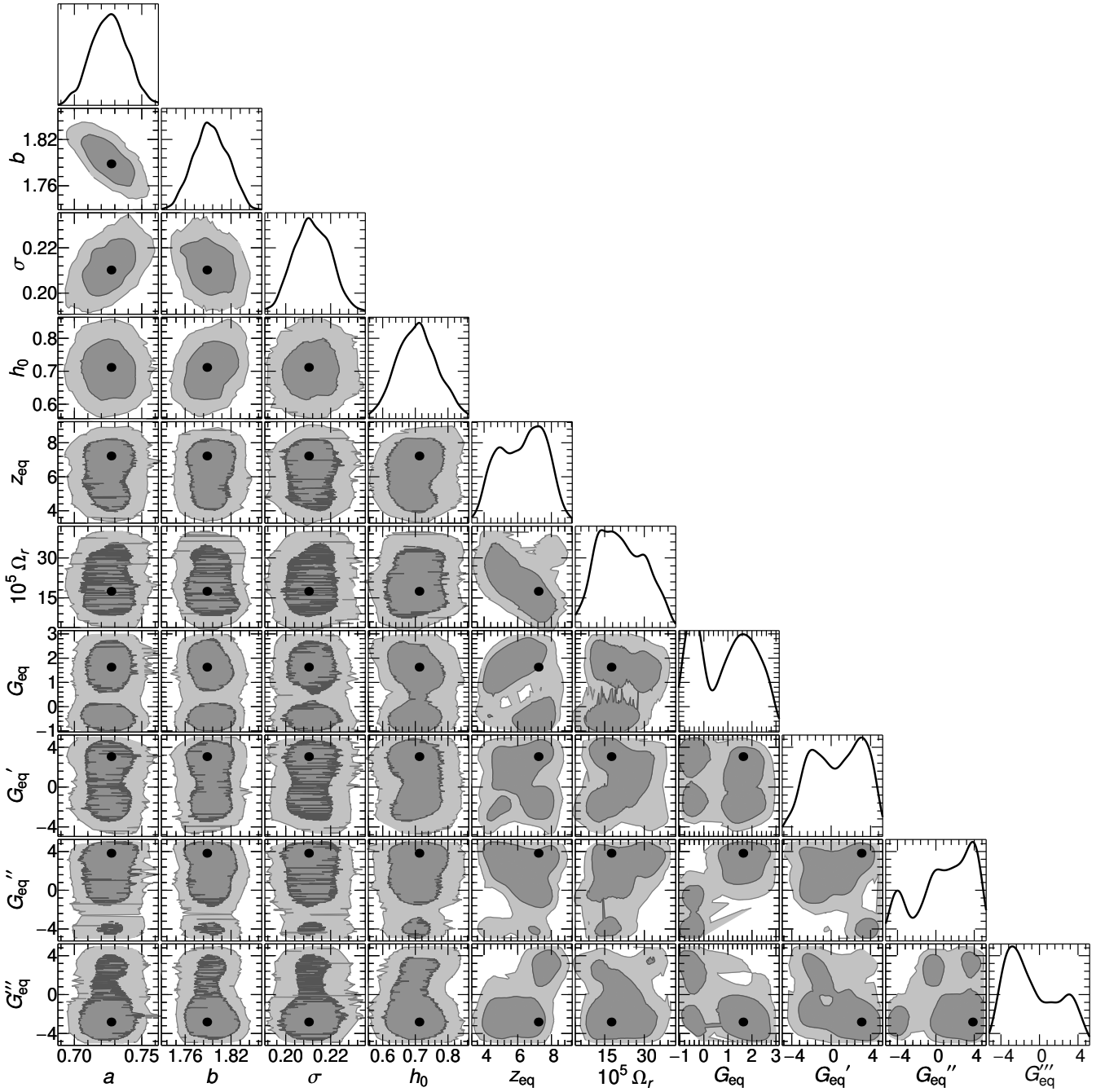


FIG. 4: Method B contour plots, got from the HBR technique, of the best-fit parameters of the E_p - E_{iso} correlation and the cosmographic approach at the dark energy – radiation equivalence. Darker (lighter) areas mark the $1\text{-}\sigma$ ($2\text{-}\sigma$) confidence regions.